HYDRO-ELASTIC NUMERIC ANALYSES OF A WEDGE-SHAPED SHELL STRUCTURE IMPACTING A WATER SURFACE

A. CONSTANTINESCU†, I. FUIOREA†, A. NEME‡, V. BERTRAM‡ and M. SALAS*

† *Military Technical Academy, Blvd. George Cosbuc 81-83, Sect. 5, RO-75275, Bucarest,Romania.*
‡ *ENSIETA, 2 rue Francois Verny, 29806 Brest Cedex 9, France.*
* *University Austral of Chile, General Lagos 2086, Valdivia Chile. msalas@uach.cl*

***Abstract*— The fluid structure interaction is simulated during the impact of a 2-d wedge on a water surface. The analysis combines the assumption of small displacements for the ideal fluid and the solid with an asymptotic formulation for accurate pressure evaluation on the wet surface boundary. Wedge deadrise angles β above approximately 30° do not fulfill this hypothesis. A fluid-heat analogy is used to obtain the regular displacement, velocity and pressure fields in the fluid domain with ABAQUS/Standard finite element code. PYTHON and FORTRAN languages are employed to connect fluid and structure data. Two methods are developed. The first method employs a weak fluid-structure coupling. The average discrepancy between our numerical results and experiments was 22% for the peak pressures for conical shell structures. The wet surface velocity was well predicted. The second method (implicit fluid-structure coupling using a convergence criterion) is more accurate. Recent results with an improved, numerical hydrodynamic model based on CFD are also presented.**

***Keywords*— Hydroelastic analysis, water impact, wedge.**

I. INTRODUCTION

The fluid-structure impact problem is important in many engineering applications. The slamming phenomenon implies, in general, very large forces because a considerable mass of water is displaced in a very short time.

Slamming is particularly important for fast ships:

- Slamming loads are often the largest loads and determine structural dimensions, particularly sensitive for light-weight, fast ships
- Even if each impact load is small, frequent impact loads accelerate fatigue failures of hulls
- Fast ships usually transport passengers and slamming loads affect passenger comfort.

A fully satisfactory theoretical treatment of slamming has been prevented so far by the complexity of the problem:

- Slamming is a strongly non-linear phenomenon which is very sensitive to relative motion and contact angle between body and free surface
- Predictions in natural seaways are inherently stochastic; slamming is a random process in reality
- Since the duration of wave impact loads is very short, hydro-elastic effects are large
- Air trapping may lead to compressible, partially supersonic flows where the flow in the water interacts with the flow in the air
- Most theories and numerical applications are for two-dimensional rigid bodies (infinite cylinders or bodies of rotational symmetry), but slamming in reality is a strongly three-dimensional phenomenon.

Bertram (2000) gives an overview of the most important analytical approaches to slamming, pointing out that in the end only computational fluid dynamics (CFD) methods are expected to bring considerable progress, while classical theories work well in two-dimensional flow for certain geometries.

We focus here on the aspect of hydro-elasticity, limiting the study to simple geometries and 2-d flows, as a first step to develop more sophisticated 3-d numerical methods.

II. MATHEMATICAL FORMULATION

We consider the problem of impact of a 3-d body on a water surface, Fig. 1. The fluid problem is formulated within potential flow theory for an ideal fluid (incompressible, inviscid and irrotational).

The velocity vector anywhere in the fluid domain follows from v = *grad* Φ. Φ(x,y,z,t) is the velocity potential. We assume small disturbances both for the solid and the fluid.

Then, the velocity potential must satisfy the following conditions:

$$\Delta\Phi = 0 \qquad \text{in } \Omega_f \tag{1}$$

$$grad\ \Phi \cdot \mathbf{n} = \dot{\boldsymbol{u}}_s \cdot \mathbf{n} = \frac{\partial \boldsymbol{u}_s}{\partial t} \cdot \mathbf{n} \qquad \text{on the wetted surface} \tag{2}$$

$$\Phi = 0 \qquad \text{on the free surface} \tag{3}$$

Equation (3) expresses the condition of zero relative pressure on the free surface. Everywhere at the free surface and at all times, the pressure corresponds to atmospheric pressure. The linearized Bernoulli equation gives then, at the free surface: $\partial\Phi/\partial t - g_z = 0$.

Neglecting gravity (wave making) for high impact speeds, we then obtain: $\partial\Phi/\partial t = 0$, thus Φ = const. As only derivatives of the potential are of interest here, we can set the constant arbitrarily to zero.

The fluid is initially at rest:

$$\Phi(x_0, y_0, z_0, 0) = 0 \tag{4}$$

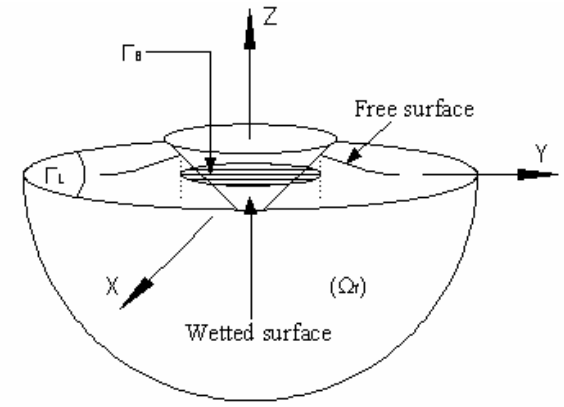

Figure 1 – Geometric definitions

The flow is not disturbed far from the body:

$$|grad\Phi| \to 0 \text{ for } (x_0{}^2 + y_0{}^2 + z_0{}^2)^{1/2} \to \infty \qquad (5)$$

Once the potential is determined, the fluid pressure is calculated by the (linearized) Bernoulli equation:

$$p = -\rho_0 \frac{\partial \Phi}{\partial t} \qquad (6)$$

The conditions on the initial water surface ($z_0 = 0$) are:

$$\frac{\partial \Phi}{\partial z_0} = \dot{u}_{sz} = \frac{\partial u_{sz}}{\partial t} \quad \text{on } \Gamma_B \qquad (7)$$

$$\Phi = 0 \quad \text{on } \Gamma_L \qquad (8)$$

$$\frac{\partial \Phi}{\partial z_0} = \frac{\partial h}{\partial t} \quad \text{on } \Gamma_L \qquad (9)$$

$$\text{where } h = \int_0^t \left.\frac{\partial \Phi}{\partial z_0}\right|_{(x,y,0,\tau)} d\tau\,, \qquad (10)$$

Γ_B is vertical projection of the body wetted surface on $z_0 = 0$, Γ_L the liquid surface, *i.e.* the free water surface, and h the instantaneous draft of the body.

An analogy to fluid-thermodynamics can be employed to solve our fluid dynamics problem with the commercial finite element code ABAQUS/Standard and its module of thermal resolution. The heat transfer model is given by the following equations:

$$\Delta T = 0 \quad \text{in } \Omega_f \qquad (11)$$

$$\lambda \frac{\partial T}{\partial z_0} = -\boldsymbol{q} \cdot \boldsymbol{z} \quad \text{on } \Gamma_B \qquad (12)$$

$$T = 0 \quad \text{on } \Gamma_L \qquad (13)$$

$$\frac{\partial h}{\partial t} = \frac{\partial T}{\partial z_0} \quad \text{on } \Gamma_L \qquad (14)$$

$$\text{where } h = \int_0^t \left.\frac{\partial T}{\partial z_0}\right|_{(x,y,0,\tau)} d\tau \qquad (15)$$

In Eq. (2), $\boldsymbol{z}$ stands for the unit vertical vector. An equivalent system to Eq.(1) and Eqs.(7)-(10) is obtained if the temperature T is expressed in [m^2/s], the thermal conductivity set to λ=1, and $\boldsymbol{q}$ expressed in [m/s] in the thermal module of ABAQUS/Standard.

In addition, it is necessary to know the extent of the wet surface d. Physically, the position of this surface is given by imposing the condition of conservation of the volume of the fluid. In an equivalent way, this condition results in finding the intersection between the rise in the free face and the position of the solid body. The rise in the free surface is expressed as the integral in time of the normal derivative of the velocity potential in Eq. (10). More simply, we can solve the problem of the displacement potential $\Psi=\Psi(x_0,y_0,z_0,t)$ such that:

$$\Psi = \int_0^t \Phi(x_0, y_0, z_0, \tau) d\tau \qquad (16)$$

and $h = \left.\frac{\partial \Psi}{\partial z_0}\right|_{(x_0,y_0,0,t)}$. Thus the potential Ψ must satisfy:

$$\Delta \Psi = 0 \quad \text{in } \Omega_f \qquad (17)$$

$$\frac{\partial \Psi}{\partial z_0} = u_{sz} \quad \text{on the wet surface} \qquad (18)$$

$$\Psi = 0 \quad \text{on the free surface} \qquad (19)$$

Again, we utilize the fluid-heat analogy to calculate the equivalent system formed by Eqs. (17-19), the temperature T will be expressed in [m^2], thermal conductivity $\lambda=1$, and $\boldsymbol{q}$ in [m] in the thermal module of ABAQUS/Standard.

III. NUMERICAL APPROACH

Donguy *et al.* (2001) developed a numerical approach to simulate 3-d slamming problems, combining the assumption of small displacements for the fluid and the solid with an asymptotic formulation for accurate pressure evaluation on the wetted surface of the body. For solving the fluid problem, they used a fluid-heat analogy under the hypothesis of incompressibility and irrotational initial velocity field for the fluid, considering the velocity potential or the displacement potential as temperature. The finite element code CASTEM was employed to determine the fluid (heat) and solid evolutions. The fluid structure interaction generates a coupling matrix which has been implemented in CASTEM.

We have globally followed the same approach using the commercial finite element code ABAQUS associated with PYTHON and FORTRAN languages instead of CASTEM. Thus, some procedures have been modified and several numerical aspects improved. The realization using ABAQUS represents one of improvements, since ABAQUS as a commercial code is widely available, not only to researchers but also to designers. In the rigid cases, we employ numerical iterations with a convergence criterion to obtain accurate values of the wet surface distances at every time increment, whereas the CASTEM approach uses a more approximate Wagner model. Concerning the hydroelastic coupling, two approaches for fluid-structure interaction have been implemented. The first one is based on an explicit resolution without global convergence criterion, the second is an implicit method associated with two global convergence criteria (strain energy for the structure and maximum peak pressure for the fluid). Donguy employed an explicit iteration followed by only one implicit at every

time increment. His method can be considered as less accurate since no convergence criterion is enforced.

We considered only wedges and cones as geometries. Three deadrise angles (6°, 10°, and 14°) between the body and the calm water surface, three initial impact velocities (2.5, 5, and 8 m/s) and three thickness values of the outer body shell (0.5, 1, and 1.5 mm) were considered.

An additional mass of 30 kg was attached in a ring around the deformable steel shells. The typical dimensions of the structure are the same as those used by Donguy *et al.* (2001) in the experiments. The pressure was measured at two points (p1 and p2), Fig. 2.

For the rigid cases, the velocity was assumed to be constant. Our simulation of the maximum pressure values agrees very well with those determined with CASTEM. We also obtain the same wet surface propagation velocity, as well as the resulting vertical force on the solid.

The study of impact with deformable structures is more complicated. A finite element method (FEM) must be employed to find the shell evolution in parallel with the fluid calculation. To couple these two simulations, we project the pressure obtained at the nodes of the fluid mesh onto the Gauss points of the solid surface and the nodal displacements or nodal velocities of the structure onto the Gauss points of the water surface. For the dihedral shells, the pressure vs. time curves exhibit discrepancies between ABAQUS and CASTEM. For the cones, the maximum pressure values are similar to those obtained experimentally (Donguy, 2002).

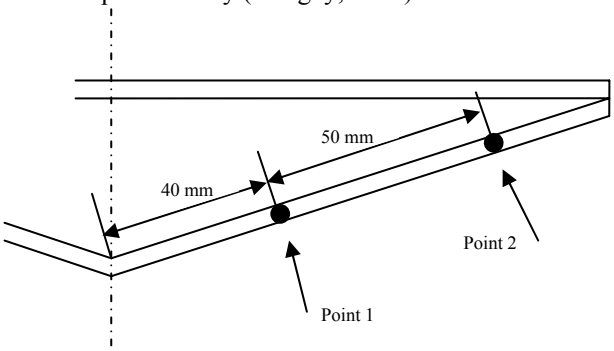

Figure 2 – Cone geometry

A. Rigid structures

We limit ourselves to two simple shapes, namely wedges and cones. Employing rotational symmetry, cones can be treated as two-dimensional bodies. The deadrise angle β of either form is defined between the body and the free surface at rest.

The two fundamental assumptions in this case are: the entry speed of the solid into the fluid is constant; the numerical time increment Δt is constant at $2 \cdot 10^{-5}$ s. The method of resolution does not require a finite element calculation, as we know exactly the position of the body surface at each time. To determine the pressure exerted by the fluid on the structure, a smaller time increment δt was used.

This time increment was optimized. A small mesh size M_s around the contact surface border is required to take into account the high potential gradient in this zone. According to the estimated wet surface velocity $\dot{d} = \frac{4}{\pi} \frac{V}{\tan(\beta)}$ for cones and $\dot{d} = \frac{\pi}{2} \frac{V}{\tan(\beta)}$ for wedges, where V is the impact velocity, δt must be greater than $M_s / \dot{d}$ to compute accurately the contact surface dimension. For $\delta t < M_s / \dot{d}$, the wetted surface border will stay within the same fluid element between t and $t + \delta t$. In this case the element interpolation order (linear) is not sufficient to give a correct value of the wetted surface dimension increment for the time increment δt. On the other hand, δt must be small enough to well determine the pressure field, Eq. (20). Finally a value of $\Delta t/3$ was retained for δt.

The calculation of the final numerical pressure in several stages (Donguy, 2002), is associated with an asymptotic development at the wetted surface boundary. This method is classically used to model the problem of the hydrodynamic impact, *e.g.* Wagner (1932). The asymptotic study led to the determination of two zones (near-field and far-field) in which two asymptotic developments are obtained then connected. Within first order, the composite solution for the pressure includes a far-field solution (fulfilling conditions far from the body-surface intersection, but being singular at the intersection) and a near-field solution (valid in the vicinity of the intersection, describing the formation of a jet). The far-field pressure is approximated by central differencing of the Bernoulli equation (20).

For the correct evaluation of the resulting total effort, it is necessary to consider also the near-field pressure, Eq. (21). For 2-d flows and very small deadrise angle (β<1°), combining near-field and far-field solutions allows to obtain an analytical so-called composite solution which is continuous in the whole domain, Eq. (22). However, in reality air-trapping occurs for such small deadrise angles, making classical potential flow approaches questionable (Bertram, 2000). Since we utilized numerical resolution and finite distances from the exact wetted surface boundary, an approximate model is necessary to connect analytical far-field and near-field pressure solutions, Eq. (23). The operating range of this connection is limited to the distance r in front of the end of wet surface.

$$p_{edfc} = -\rho_f \frac{\Phi^{t_j} - \Phi^{t_j - \delta t_j}}{\delta t_j} \tag{20}$$

$$p_i(x_0, t) = \rho_f \frac{\dot{d}^2}{2} \left[1 - \left(\frac{1-u}{1+u} \right)^2 \right], \quad u \in [0,1]$$

$$x_0 - d(t) = \frac{\delta\delta(t)}{\pi} \left(-2\ln u - \frac{4}{u} - \frac{1}{u^2} + 5 \right) \text{for } x_0 < d(t) \tag{21}$$

$$x_0 - d(t) = \frac{\delta\delta(t)}{\pi} \left(-2\ln u - 4u - u^2 + 5 \right) \text{for } x_0 > d(t)$$

$$\delta\delta(t) = \frac{\pi}{8}\frac{V^2 d(t)}{\dot{d}^2(t)}$$

$$(p_i)_e(x_0,t) = \rho_f \frac{V d\,\dot{d}}{\sqrt{2d(d-x_0)}} \qquad (22)$$

$$(p_i)_e^{num}(x_0,t) = (p_i)_e(x_0,t) \;\; for \;\; x_0 < d - r(t)$$

$$(p_i)_e^{num}(x_0,t) = \frac{(p_i)_e(x_0,t) - p_{edfc}}{r(t)}(d-x_0) + p_{edfc} \;\; for \;\; x_0 > d - r(t) \qquad (23)$$

In these expressions, ρ_f stands for the fluid density, taken as 1000 kg/m^3 for fresh water. The final pressure is given by the composite numerical corrected pressure:

$$p_{num} = p_{edfc} + p_i - (p_i)_e^{num} \qquad (24)$$

From these previous set of equations we can prove that the maximal pressure equals to:

$$\rho_f \frac{\dot{d}^2}{2} \qquad (25)$$

As in the drop tests of Donguy (2002), we calculated with CASTEM and ABAQUS the time histories of the pressure at the two points p_1 and p_2, at a distance of 40 mm and 90 mm, respectively, of the top of the body, Fig. 3.

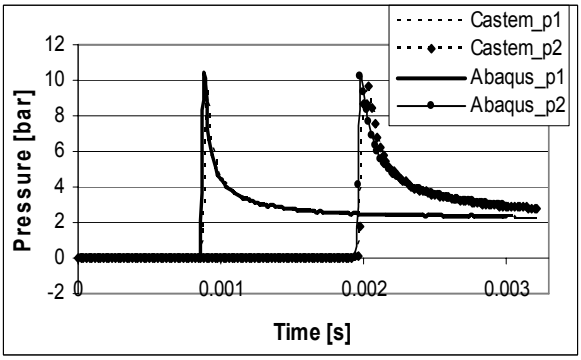

Figure 3 – Pressure vs. time at points p_1 and p_2 for cone of 6° deadrise and impact velocity 5 m/s

The results obtained with ABAQUS and CASTEM were very similar and in good agreement with analytical solutions following Wagner, Zhao and Faltinsen. The similarity of the results may obscure the difference of the quality between the two codes. The main difference refers to the calculus of the wet surface extent d. Donguy uses sometimes an analytical formulation, whereas ABAQUS employs an iterative process with a convergence criterion. In conclusion, those satisfactory results have permitted to bring a first validation to our code and they allowed the continuation of the simulations in the deformable case. The latter exhibits more discrepancies between the two approaches.

For rigid cones, the results were also satisfactory. Table I compiles the maximum values of the pressures for various configurations. The maximum values calculated with ABAQUS are very close to those given with CASTEM. Both differ from experimental values, because the sensors average the pressure over the sensor area. Averaging our numerical results over the sensor area gives then also much better agreement with experiments.

Table I: Pressures [bar] on rigid cone for deadrise angle 10°

Speed	2.5 m/s		5 m/s	
Position	p_1	p_2	p_1	p_2
ABAQUS	1.67	1.68	6.7	6.7
CASTEM	1.6	1.6	5.4	6.6
Experiment	1.0	1.4	4.1	5.6
ABAQUS averaged	1.12	1.6	4.5	5.6

The time history of the force as function of deadrise angle is very close to that obtained with CASTEM, as well as with the analytical non-linear solution determined by Zhao and Faltinsen (1992). The peak pressure obtained by Zhao and Faltinsen corresponds to the analytical expression derived by combining Eq. (24) with the expressions for the wet surface velocity for cones and wedges given above:

$$\frac{\rho_f}{2}\left[\frac{4}{\pi}\frac{V}{\tan(\beta)}\right]^2 \qquad \text{for cones} \qquad (26)$$

$$\frac{\rho_f}{2}\left[\frac{\pi}{2}\frac{V}{\tan(\beta)}\right]^2 \qquad \text{For wedges} \qquad (27)$$

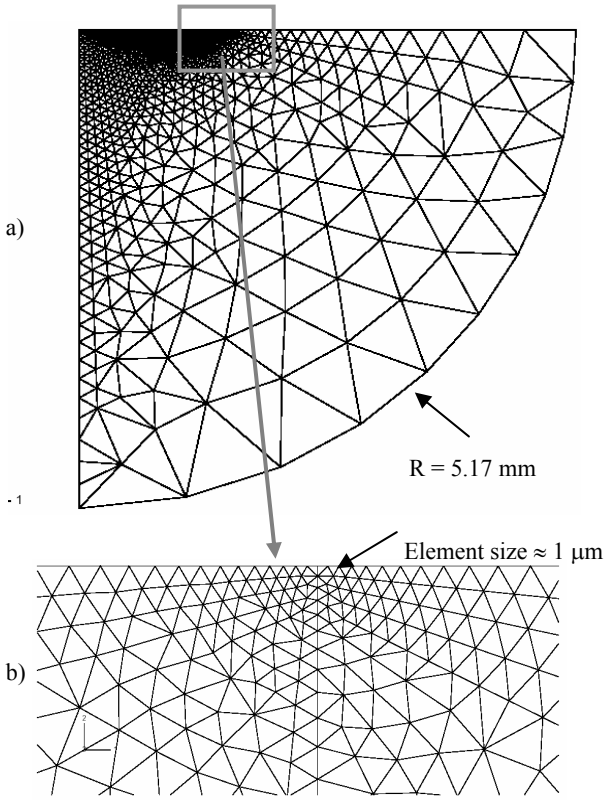

Figure 4 – Fluid mesh at the first increment (20μs),m for a 6° cone impacting the water surface at 4 m/s a) complete mesh, b) big zoom on 'a'

We optimized the fluid mesh reducing the number of elements successively while checking that the results still agreed with equations (26) and (27), respectively. Without apparent loss of accuracy in results, we thus reduced the mesh size from initially 30000 linear triangular elements to 2000, Fig. 4. The zone with a fine grid

corresponds to the intersection between the fluid surface and the body surface. The drastic reduction in elements resulted in a much smaller, but still considerable reduction in CPU time by a factor 2.

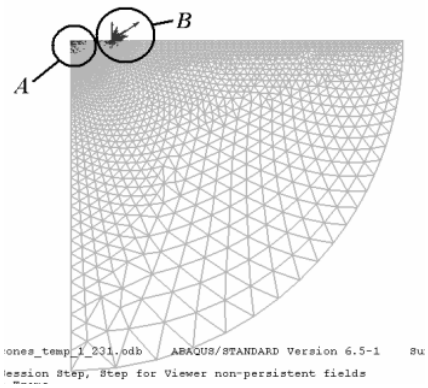

Figure 5 – Vertical velocity at the first increment (20μs), for a 6° cone impacting the water surface at 4 m/s

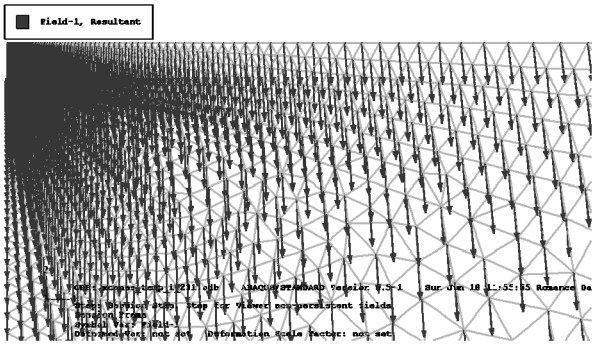

a) Detail of the zone A (velocity gradient)

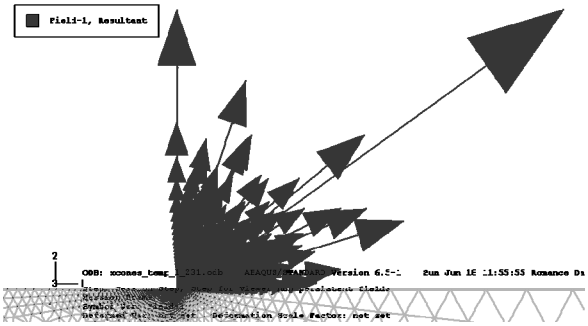

b) Detail of the zone B (velocity gradient)

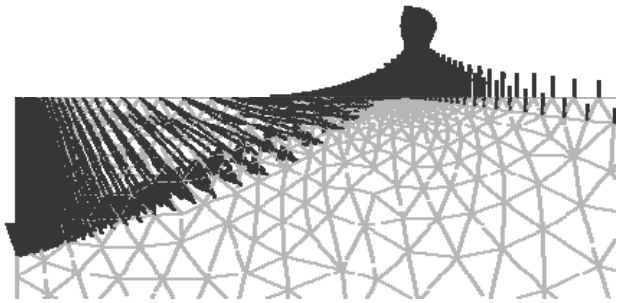

c) Displacement gradient

Figure 6 – Velocity and displacement vectors at the first increment (20μs), for a 6° cone impacting the water surface at 4 m/s

a)

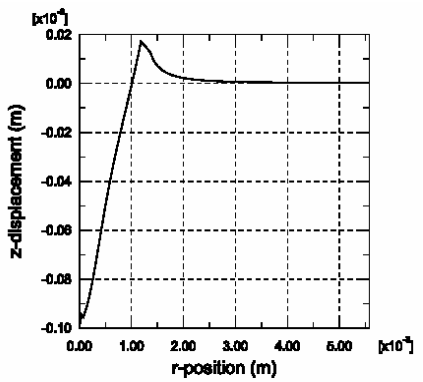

b)

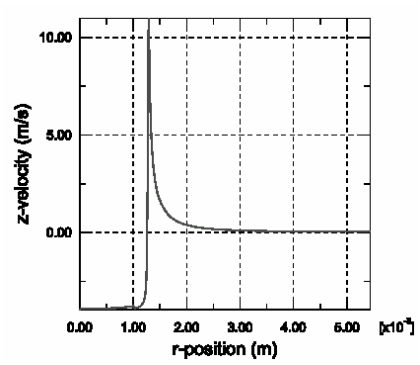

c)

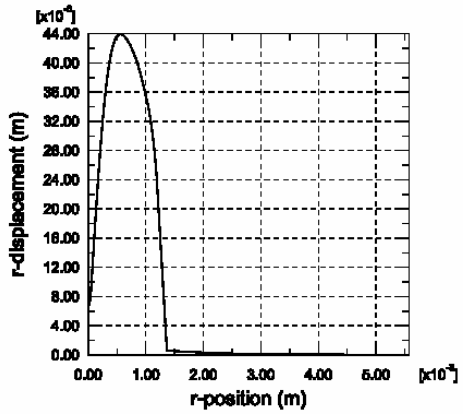

d)

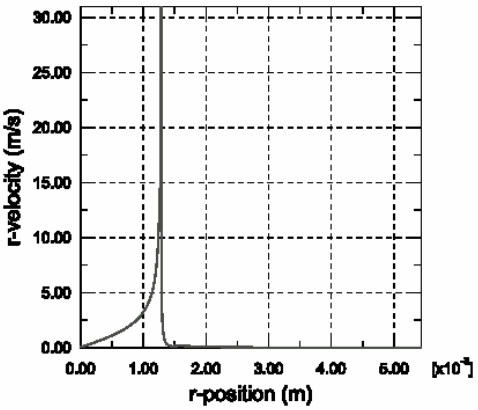

Figure 7 – Values extrapolated at water surface nodes corresponding to the first increment (20μs), for a 6° cone impacting the water surface at 4 m/s, of a) vertical displacement, b) vertical velocity, c) radial displacement d) radial velocity

The reason is that the pressure interpolation between fluid and structure nodes depends on the number of elements on the body contour, not on the elements on the free surface. Also, the number of necessary iterations to determine the wetted surface increases as the mesh becomes coarser.

The dimension of the meshed fluid zone is adapted to the contact surface between solid and water. Figure 5 shows that the velocity vanishes within the furthest elements as it must be.

The mesh refinement, around the intersection between the fluid surface and the body surface, allows to capture the high velocity gradient (Fig. 6, a, b) and the displacement gradient (Fig. 6, c).

We can also check after post-processing if the Neumann condition (no penetration) is correctly prescribed along the contact line between solid and fluid, Fig. 7.

B. Deformable Structures

The impact study of deformable structures is more complicated as it requires simultaneous computations of fluid and structure. The flow computations remain very similar to the rigid body case, but the structure calculation and its coupling to the fluid calculation differ considerably between our approach using ABAQUS and Donguy's (2002) approach using CASTEM. Donguy used a strong fluid-structure coupling iterative process - only two iterations - during the time step Δt.

Our method associates in a sequential manner both the fluid and the structure developments, at every step of the process, without convergence criteria (Fig. 8). The fluid-structure coupling is explicit since the constant pressure at time t_i is applied for the dynamic deformable structure simulation between t_i and t_{i+1}. We employ the *RESTART function of ABAQUS. This command allows to stop and to restart a simulation without losing the history of the positions, velocities and accelerations at nodes. During the resulting pauses, we carry out a fluid calculation. Thus an explicit integration, denoted here 'ping-pong scheme', is achieved in our case. This method does not represent a true improvement over Donguy's approach, but it allows us to have a first representation of the fluid-structure coupling.

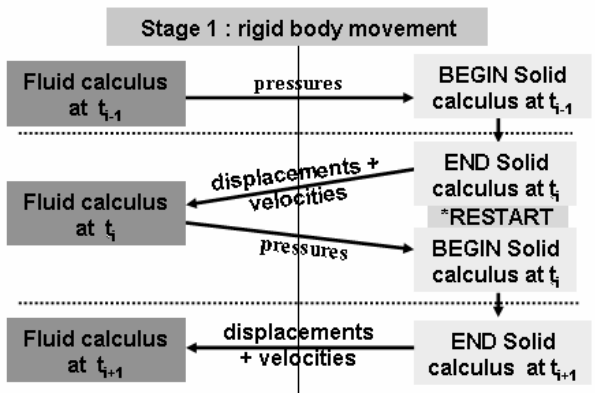

Figure 8 – Ping-pong scheme

Fluid pressures and position of the body are expressed by values at the nodes. Because the fluid grid does not coincide with structure grid, we use a cubic spline to interpolate pressures from the fluid grid to the structure grid (Gauss points) and displacements and velocities from the structure grids to the fluid grid. Compared to the rigid case, in the deformable case we record important differences for the wedge between the two approaches, ABAQUS and CASTEM. For instance, the pressure p_1 obtained with CASTEM is 2.7 bars and 11.5 bars with ABAQUS for velocity 5 m/s, shell thickness 1 mm and deadrise angle 6º.

For cones, the results between the two approaches agree qualitatively well, Fig. 9. A reliable quantitative comparison is impossible because not all details were documented in Donguy (2002). Moreover, the experimental peak pressures at p1 and p2 exhibit dispersion (*e.g.* around 40 % with 1 mm thick aluminum cone, deadrise angle 6º, impact velocity 2,5 m/s). According to Peseux (2003), comparisons between numerical and experimental results as well as descriptions of the pressure distribution on elastic structures are a challenge. The maximum values of the pressures decrease less over time (compared to values obtained with the wedge) due to the relatively larger rigidity of cones.

We tried to improve our explicit fluid-structure interaction scheme. We went further than Donguy's model by computing a totally implicit fluid-structure interaction. The main idea is to calculate alternatively up to the complete plunging of the structure into water both the time history of displacement and velocity of the structure nodes, and the fluid pressure time history along the contact surface for prescribed deformation. This iterative process starts with the flow computation, considering a rigid body motion for the solid.

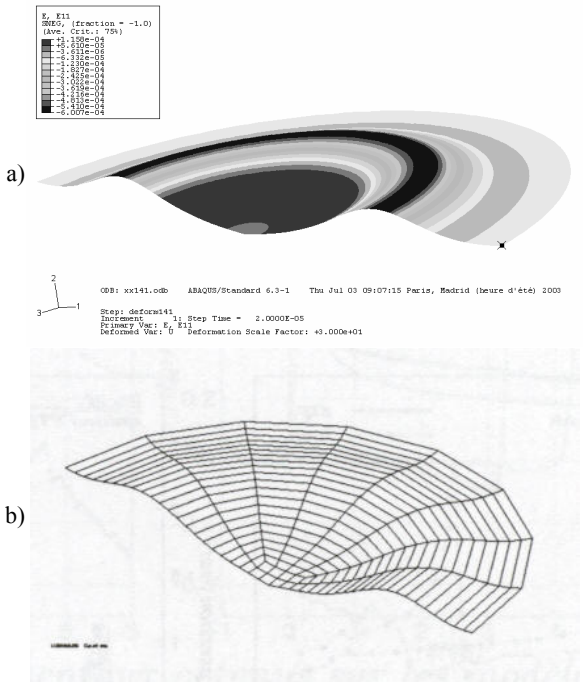

Figure 9 – Scaled deformation of a cone: ABAQUS (a) and CASTEM (b)

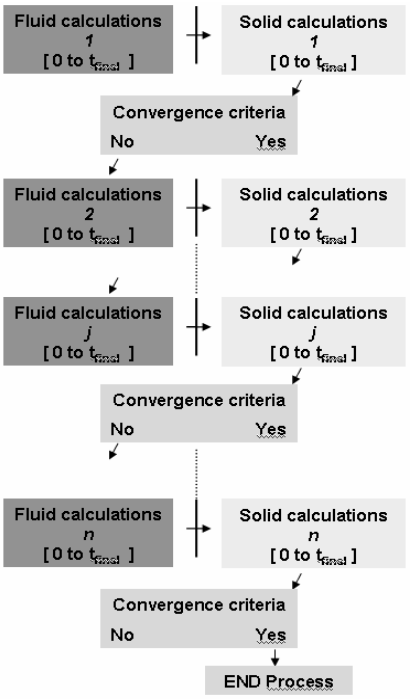

Figure 10 – Process scheme

The obtained fluid pressure time history along the contact surface is transferred to the transient dynamic finite element analysis of the structure. The post-processing of this finite element analysis allows to determine the time history of displacement and velocity of the structure nodes which it is transferred to the fluid finite element analysis, and so on. This iterative scheme, denoted here 'process scheme', is carried on until convergence (Fig. 10). The implicit feature of the fluid-structure coupling is justified by the fact that the constant pressure at time t_{i+1} (t_i with "ping-pong" scheme) is applied for the dynamic deformable structure simulation between t_i and t_{i+1}.

We conducted the simulation of a 6º cone impacting the water surface at 4 m/s. The structure was 1.5 mm thick. The cone meridian was 16 cm long. We made the assumption of elastic behavior for the material (steel) with a Young modulus 210 GPa, a Poisson ratio 0.3, and a density 7800 kg/m^3. Figure 11 represents the peak pressure distribution along the solid structure after the 134th and the 135th of the implicit iterative process. More loops are necessary to obtain the convergence over 0.12 m of wet surface. For this method time calculation becomes long, but there is a possibility of reducing the CPU time. Thus, for the improvement of the computing time, we will cut out the total time of analysis in great intervals of time. We will carry out calculation of process until convergence independently on each great interval of time.

Figure 12 compares our explicit 'ping-pong' and implicit 'process' fluid-structure interaction schemes. The explicit 'ping-pong' scheme and the final iterations of the implicit scheme yield similar results. The apparent wiggles may be due to numerical instabilities, but also due to vibrations of the body.

We have improved the procedure by limiting the CPU time (reduction factor around 0.01). The idea was to compute the iterations and the convergence criterion at each time increment Δt instead of the total time [0, t_{final}]. We compared this new approach to the ping-pong scheme and the CASTEM procedure (Fig. 13). The maximal discrepancy is around 10 % between our implicit coupling method and the CASTEM results. Even if there are no reliable experiment to classify the different models, we argue that an implicit procedure with convergence criterion should be more appropriate than a simple approach with one explicit iteration followed by one implicit iteration.

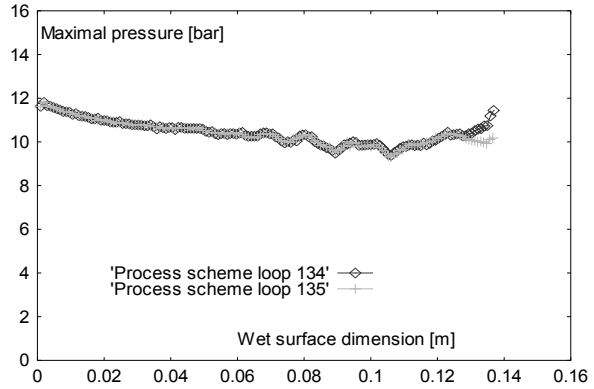

Figure 11 – Maximal pressure distribution after different loops of the process scheme

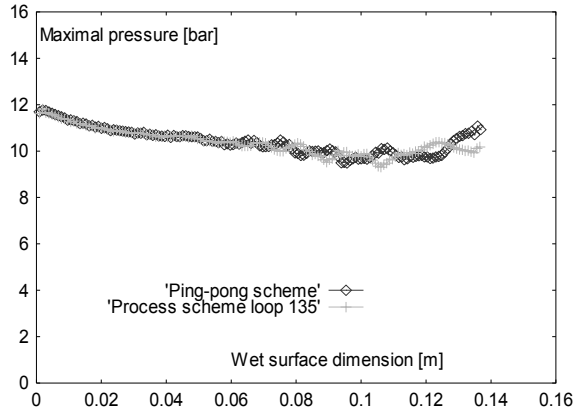

Figure 12 – Maximal pressure distribution; process scheme and ping-pong scheme

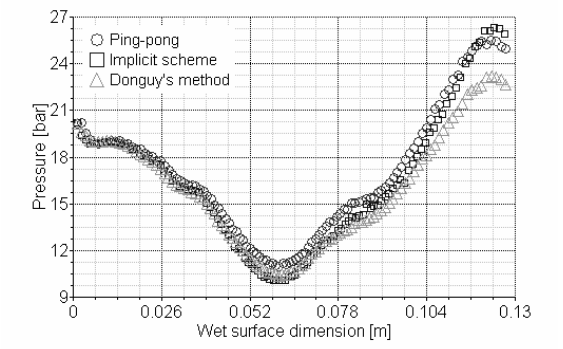

Figure 13 – Maximal pressure distributions. Wedge shape 2 mm thick hull impacting a water surface with a 14° deadrise angle.

IV. FIRST STUDIES FOR AN IMPROVED HYDRODYNAMIC MODEL

For most practical impact problems, the body shape is complex and the effect of gravity is considerable. In such cases, analytical solutions are very difficult or even impossible. This leaves CFD as a tool for further improvement in the hydrodynamic modeling of the problem. Various researchers have approached slamming problems, usually employing surface capturing-methods, e.g. Volume-of-Fluid or level-set techniques. See Bertram *(*2000) for a discussion of these various CFD techniques. Although viscosity plays a less important role for slamming than for many other problems in ship hydrodynamics, usually RANSE (Reynolds-averaged Navier-Stokes equations) solvers were employed, *e.g.* Muzaferija and Peric (1998), Muzaferija *et al.* (1998), Fig. 14; Sames *et al.* (1998), Fig. 15;, and most noteworthy for planing hulls Caponnetto (2002). To investigate the hydroelastic response of a monohull, Salas (2001) employed 3d hydrodynamics to predict body motions and 2d formulae to predict impact pressures.

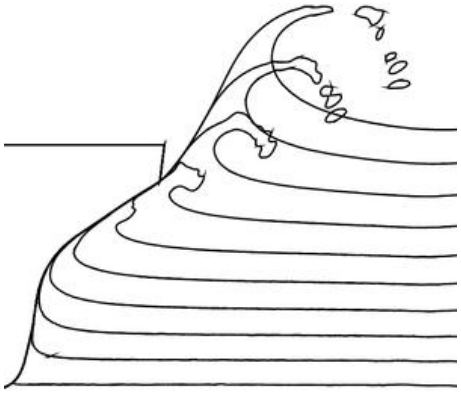

Figure 14 – 2D Slamming simulation using CFD, Muzaferija *et al.* (1998).

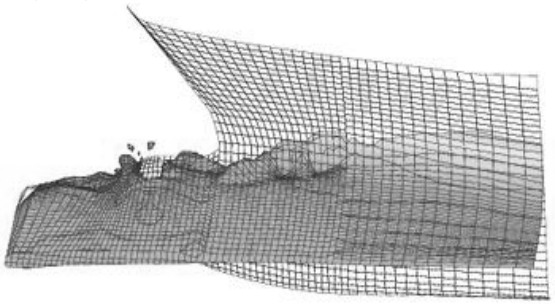

Figure 15 – 3D slamming simulation using CFD, Sames *et al.* (1998).

Our hydrodynamic model is so far insufficient for practical work, as it is fundamentally limited to 2-d and even there to a narrow bandwidth of deadrise angles. While the approach was justified by advancing more rapidly on the fluid-structure interaction aspect and testing the ABAQUS software, we will eventually use CFD methods to model the fluid aspects.

In cooperation with the Sharif University/Tehran, we reproduced the complex free-surface deformation with detaching jet and droplets for the water entry of a wedge with deadrise angle 30º, both for the symmetric case and the case of the wedge tilted by 10º, Fig. 16, Seif *et al.* (2005). In this case, we employed the commercial RANSE solver Fluent in version 6.0.

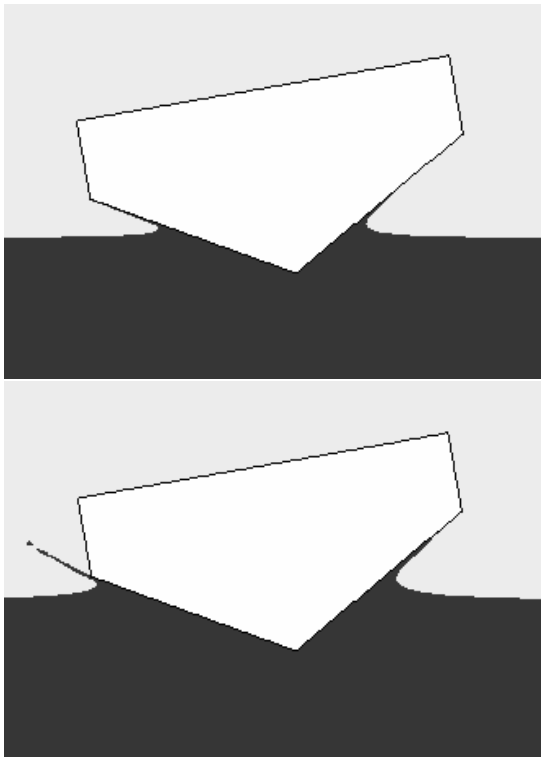

Figure 16 – Water surface deformation for wedge with deadrise angle β=30° computed with Fluent

V. CONCLUSIONS

For the rigid-body water entry, the hybrid fluid-structure approaches based on CASTEM and ABAQUS give practically identical results for the propagation velocities of the wetted surface and differences in pressure of approximately 5%. Numerical values for maximum pressures are higher than measured due to the averaging effect of finite sensor areas. Analytical results obtained by Zhao and Faltinsen (1992) for the evolution of the non-dimensionalized expression (f), Eq. (28), associated to the force per unit length (F), as function of time (t), deadrise angle (β), and entry speed (V) were well reproduced by our approach (Fig. 17).

$$f = \frac{F \tan^2 \beta}{\rho_f V^3 t} \tag{28}$$

For the deformable body case, differences between ABAQUS and CASTEM are larger, undoubtedly related to the differences in modeling. In general, the time steps for the deformations are similar between the two codes. Note that partially plastic deformation was observed for the cone and the wedge with 6º deadrise in experiments.

There is general consensus for the need of proper validation for numerical slamming simulations. A shock machine allowing controlled water entry velocity and hydro-elastic detailed pressure measurements will help to validate CFD simulations, finding suitable grid and other input parameters for quasi-3d cases like cones.

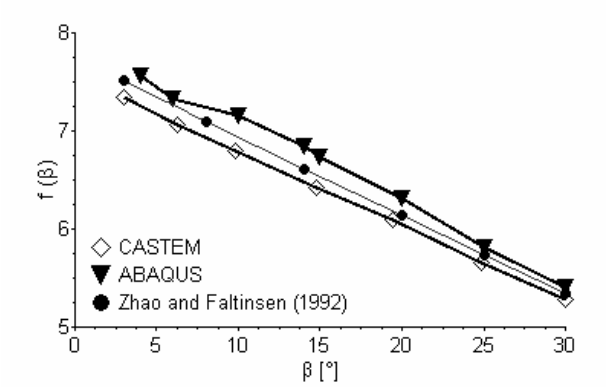

Figure 17 – Evolution of the force as function of deadrise angle in the case of the wedges.

NOMENCLATURE

T temperature (m^2/s or m^2)
Γ_L free surface (m)
Γ_B vertical projection of the body wetted surface (m)
Δt numerical time increment
Φ velocity potential of fluid (m^2/s)
Ψ displacement potential of fluid (m^2)
p fluid pressure (N/m^2)
u_s displacement of the structure (m)
q heat flux (m/s or m)
β deadrise angle
λ thermal conductivity
ρ_f fluid density (kg/m^3)

ACKNOWLEDGEMENTS

We are grateful for discussions and encouragement from Bernard Peseux (ECN, Nantes) and Yann Doutreleau (ENSIETA, Brest), Mohammad Seif (Sharif Univ., Tehran) for supplying initial grids for the CFD computations.

REFERENCES

Bertram, V., *Practical Ship Hydrodynamics*, Butterworth+Heinemann, Oxford (2000).

Caponnetto, M., "Sea keeping simulation of fast hard chine vessels using RANSE," *NuTTS 02*, Pornichet (2002).

Donguy, B., B. Peseux, B. and F. Fontaine, "Numerical and experimental investigation of a rigid cone striking the free surface of an incompressible fluid," *ASME, PVP Conf.*, Atlanta (2001).

Donguy, B., *Study of the fluid interaction structure at the time of the hydrodynamic impact*, Doctoral Thesis, Ecole Centrale de Nantes, France (2002).

Muzaferija, S. and M. Peric, "Computation of free-surface flows using interface tracking and interface-capturing methods," *Nonlinear Water Wave Interaction*, Comp. Mech. Publ., 59-100 (1998).

Muzaferija, S., M. Peric, P. Sames and T. Schellin, "A two-fluid Navier-Stokes solver to simulate water entry," *22nd Symp. Naval Hydrodyn.*, Washington (1998).

Peseux, B., L. Gornet and B. Donguy, "Hydrodynamic impact: Numerical and experimental investigations", *Journal of Fluids and Structures*, **21**, 277–303 (2005).

Salas, M., "Hydroelastic Simulation of Slamming Loads" *4th Numerical Towing Tank Symposium* (NuTTS'01), Hamburg, (2001)

Sames, P.; T. Schellin, S. Muzaferija and M. Peric, "Application of two-fluid finite volume method to ship slamming," *OMAE'98*, Lisbon (1998).

Seif, M.S., S.M. Mousaviraad, S.H. Saddathosseini and V. Bertram, "Numerical modeling of 2-d water impact in one degree of freedom," *Síntesis Tecnológica,* **2**, 79-84 (2005).

Wagner, H., "Über Stoβ- und Gleitvorgänge an der Oberfläche von Flüssigkeiten," *Zeitschrift für Angewandte Mathematik und Mechanik*, **12**, 193-215 (1932).

Zhao, R. and O. Faltinsen, "Slamming loads on high-speed vessels," *19th Symp. Naval Hydrodyn.*, Seoul, Korea (1992).

Received: January 19, 2006.
Accepted: January 15, 2007.
Recommended by Subject Editor Alberto Cuitiño.